Article

Immunity

T Follicular Helper Cells Have Distinct Modes of Migration and Molecular Signatures in Naive and Memory Immune Responses

Graphical Abstract

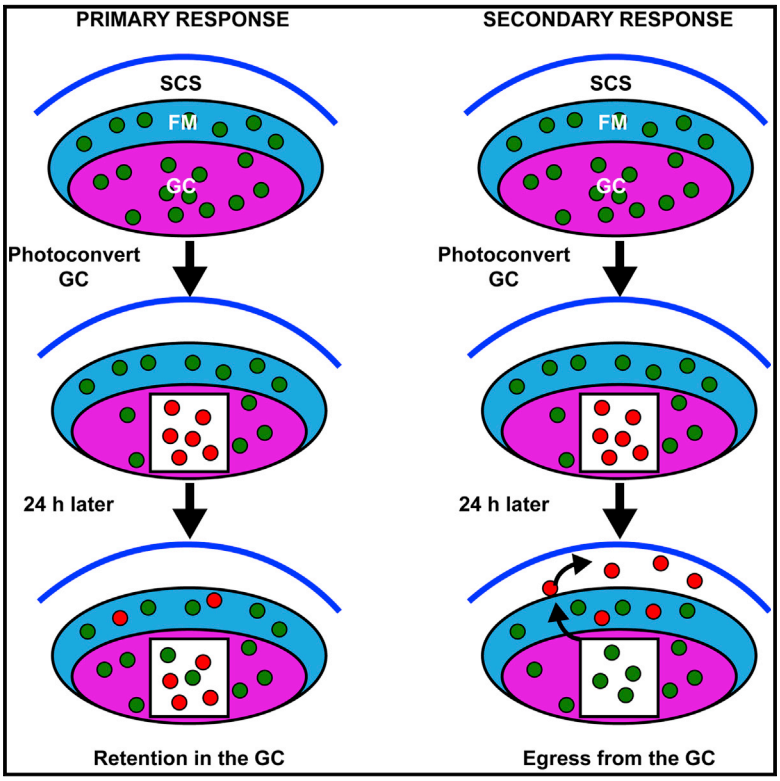

Authors

Dan Suan, Akira Nguyen, ..., Tatyana Chtanova, Tri Giang Phan

Correspondence

t.chtanova@garvan.org.au (T.C.), t.phan@garvan.org.au (T.G.P.)

In Brief

This study shows that Tfh cells are confined to the germinal center (GC) in the primary response and that follicular memory T cells are reactivated and proliferate in the subcapsular region. It also shows that Tfh cells are able to egress from the follicle in the secondary response.

Highlights

- Primary Tfh cells are confined to the germinal center
- Follicular memory T cells scan subcapsular sinus macrophages for antigen
- Secondary Tfh cells are reactivated and proliferate in the subcapsular region
- Secondary Tfh cells egress from the follicle via the subcapsular sinus

Suan et al., 2015, Immunity *42*, 704–718
April 21, 2015 ©2015 Elsevier Inc.
http://dx.doi.org/10.1016/j.immuni.2015.03.002

CellPress

Immunity
Article

T Follicular Helper Cells Have Distinct Modes of Migration and Molecular Signatures in Naive and Memory Immune Responses

Dan Suan,[1,2,6] Akira Nguyen,[1,2,6] Imogen Moran,[1,2,6] Katherine Bourne,[1] Jana R. Hermes,[1] Mehreen Arshi,[1,3] Henry R. Hampton,[1,2] Michio Tomura,[4] Yoshihiro Miwa,[5] Anthony D. Kelleher,[3] Warren Kaplan,[1,2] Elissa K. Deenick,[1,2] Stuart G. Tangye,[1,2] Robert Brink,[1,2] Tatyana Chtanova,[1,2,*] and Tri Giang Phan[1,2,*]

[1]Garvan Institute of Medical Research, 384 Victoria Street, Darlinghurst, NSW 2010, Australia
[2]St Vincent's Clinical School, Faculty of Medicine, UNSW Australia, 390 Victoria Street, Darlinghurst, NSW 2010, Australia
[3]St Vincent's Centre for Applied Medical Research, 405 Liverpool Street, Darlinghurst, NSW 2010 Australia
[4]Kyoto University Graduate School of Medicine, Yoshida-honmachi, Sakyo-ku, Kyoto 606-8501, Japan
[5]University of Tsukuba, Ibaraki Prefecture, Tsukuba 305-8572, Japan
[6]Co-first author
*Correspondence: t.chtanova@garvan.org.au (T.C.), t.phan@garvan.org.au (T.G.P.)
http://dx.doi.org/10.1016/j.immuni.2015.03.002

SUMMARY

B helper follicular T (Tfh) cells are critical for long-term humoral immunity. However, it remains unclear how these cells are recruited and contribute to secondary immune responses. Here we show that primary Tfh cells segregate into follicular mantle (FM) and germinal center (GC) subpopulations that display distinct gene expression signatures. Restriction of the primary Tfh cell subpopulation in the GC was mediated by downregulation of chemotactic receptor EBI2. Following collapse of the GC, memory T cells persisted in the outer follicle where they scanned CD169$^+$ subcapsular sinus macrophages. Reactivation and intrafollicular expansion of these follicular memory T cells in the subcapsular region was followed by their extrafollicular dissemination via the lymphatic flow. These data suggest that Tfh cells integrate their antigen-experience history to focus T cell help within the GC during primary responses but act rapidly to provide systemic T cell help after re-exposure to the antigen.

INTRODUCTION

The production of neutralizing antibodies by long-lived plasma cells and memory B cells upon antigen re-exposure underpins the protection afforded by most successful vaccines (Plotkin, 2008). These outputs from the germinal center (GC) are critically dependent on sequential CD4$^+$ T cell help provided to B cells at multiple sites including the interfollicular zone (Kerfoot et al., 2011), T-B border (Garside et al., 1998; Okada et al., 2005), and within GCs (Allen et al., 2007; MacLennan, 1994; Victora and Nussenzweig, 2012) to drive antibody affinity maturation and memory formation (Crotty, 2011). The term follicular B helper T cells (Tfh) was originally used to describe human CD4$^+$ T cells that express the chemokine receptor CXCR5, localize to the secondary follicle of tonsils, and provide cognate help to B cells (Breitfeld et al., 2000; Schaerli et al., 2000). The importance of Tfh cells to human health is underscored by the recurrent bacterial infections that occur when they are defective, and the autoimmune pathologies that develop when they are in excess (Tangye et al., 2013). Rapid developments in the Tfh field in recent years has been facilitated by the use of cell surface molecules, such as CXCR5, PD-1, and ICOS (Haynes et al., 2007; Rasheed et al., 2006), as surrogate markers for tracking Tfh cells in human subjects and genetic mouse models. Unfortunately, these markers of CD4$^+$ T cell activation are not unique to Tfh cells. For example, CXCR5 is upregulated by multiple CD4$^+$ T cell lineages upon activation in vivo (Ansel et al., 1999; Schaerli et al., 2001). Nevertheless, the recognition that the transcriptional repressor Bcl-6 is absolutely required for Tfh cell development firmly established them as a distinct CD4$^+$ T cell lineage (Chtanova et al., 2004; Johnston et al., 2009; Nurieva et al., 2009; Yu et al., 2009). However, Bcl-6 expression is also not Tfh cell-specific as it is upregulated in all dividing CD4$^+$ T cells during their interactions with dendritic cells (DCs) (Baumjohann et al., 2011; Kitano et al., 2011). Taken together, these uncertainties make it difficult to conclusively track the origin and fate of Tfh cells in the primary and secondary antibody response.

Recently, a method for in vivo photoactivation of cells expressing PA-GFP in precise microanatomical compartments was described (Victora et al., 2010), which makes it possible to optically mark Tfh cells and track them 20 hr later (Shulman et al., 2013). Unexpectedly, it was reported that Tfh cells frequently migrated out of the follicle to invade neighboring GCs and proposed that this promoted affinity maturation by providing a diverse polyclonal source of CD4$^+$ T cell help (Shulman et al., 2013). However, the temporospatial context of such promiscuous behavior was not defined. We have developed an alternative method for optical marking by two-photon photoconversion (TPP) of cells expressing the photoconvertible fluorescent protein Kaede (KD) (Chtanova et al., 2014). Our studies using TPP show striking differences in the migration and behavior of Tfh cells during three distinct phases: the primary response by naive CD4$^+$ T cells; the memory phase following resolution of the GC response; and the secondary response by

antigen-experienced cells. We demonstrate the migration of GC Tfh cells in the primary response was confined to the GC of origin and infrequently observed to cross into the follicular mantle (FM), a distinct region in the follicle surrounding the GC (Hardie et al., 1993). Follicular memory T cells were tracked to the outer follicle where they scanned $CD169^+$ macrophages lining the subcapsular sinus (SCS) and became activated to divide upon antigen rechallenge. There was unrestricted movement of GC Tfh cells in the secondary response, and we show that they also enter and leave the follicle via the lymphatic flow in the SCS. Finally, we use TPP and single cell gene expression and functional analyses to show that the temporospatial cues guiding the positioning of Tfh cells during these phases of the immune response were provided in part by Epstein-Barr virus-induced G protein coupled receptor 2 (EBI2).

RESULTS

Spatial Segregation of Primary Tfh Cells in the FM and GC

To track Tfh cells, we adoptively transferred KD OT2 $CD4^+$ T cells into recipient mice deficient for SLAM-associated protein (SAP) (Czar et al., 2001), and immunized them subcutaneously with chicken ovalbumin (OVA). The expansion of $CXCR5^+CCR7^{lo}$ $PD\text{-}1^+$ cells in the draining lymph node was used to track Tfh cell kinetics and this peaked on day 5, 2 days before the peak of GC B cells (Figure S1). Similar kinetics were observed in wild-type recipient mice (Figure S1). This was confirmed by histology and FACS analysis of optically marked cells, which showed that the follicle is extensively colonized by $CXCR5^+$ $CCR7^{lo}PD\text{-}1^+$ Tfh cells on day 5, before mature GCs have formed (Figure S2 and data not shown). Previously we labeled follicular stromal cells in vivo by injecting anti-CD157 mAb the day before imaging (Phan et al., 2007). We now report that anti-CD157 injected subcutaneously 3–4 days prior to imaging results in redistribution of the anti-CD157 label such that it also colocalizes with IgD^{lo} antigen-specific GC B cells, peanut agglutinin (PNA), CD35, and FDC-bearing immune complexes. This CD157-rich region excludes IgD^+ naive B cells and polyclonal B cells, consistent with classical definitions of GCs (see Figure S3 and Supplemental Experimental Procedures for description and validation of the labeling strategy). Time-lapse microscopy of the lymph node at the peak of the primary GC response on day 7 showed Tfh cells were localized in two separate microanatomical compartments within the follicle (Figures 1A and 1B and Movie S1). Thus, some Tfh cells were confined to the GC (i.e., GC Tfh cells) and only infrequently observed to emigrate from the GC to the FM (<10%). Other Tfh cells were confined to the FM, and these FM Tfh cells were similarly observed to cross over into the GC at a low frequency (<20%). Cell tracking showed that both GC and FM Tfh cells were highly motile with median instantaneous velocities of 8.5 and 7.8 μm/min and median confinement indices of 0.41 and 0.47, respectively (Figures 1C and 1D). This spatial confinement was confirmed by intravital TPP and discontinuous tracking of the same GC 24 hr later, which showed that ~65% of photoconverted GC Tfh cells were retained in the original GC and ~33% had migrated into the FM of the original follicle (Figures 1E–1G and Movie S2). In contrast to the findings of Shulman et al., >98% of the photoconverted GC Tfh cells were retained in the original follicle, and only a few cells could be found outside in immediately adjacent GCs (see yellow triangles in Figure 1E).

Primary GC and FM Tfh Cells Have Distinct Gene-Expression Signatures

Lymph nodes were then harvested on day 7 and multiple areas in either the GC or FM photoconverted ex vivo (Figures 2A and 2B). FACS analysis of photoconverted red cells showed both populations expressed high amounts of CXCR5 and PD-1 and low amounts of CCR7 (Figures 2C and 2D). However, while GC Tfh cells had 2-fold higher expression of CXCR5 and PD-1 than FM Tfh cells, there was overlap in the amount of protein expressed, making it difficult to exclusively resolve them by FACS (Figures 2C and 2D). These data show primary GC and FM Tfh cells are anatomically distinct Tfh subpopulations that are best resolved by location-based optical marking rather than CXCR5 and PD-1 expression.

To further characterize these unique primary Tfh cell subpopulations, we optically marked them and performed multiplex single cell RT-qPCR on day 7 for expression of a panel of 32 genes in 64 GC and 62 FM Tfh cells (Figure S4). Seven of the 32 genes included as negative controls (*Foxp3*, *Il2ra*, *Infg*, *Prdm1*, *Rorc*, *Slamf8*, and *Tbx1*) were not expressed by any of the Tfh cells and were therefore excluded from analysis. GC Tfh cells expressed >2-fold higher of *Bcl6*, *Pdcd1*, *Rgs16*, *Il21*, and *Il4* transcripts and >2-fold lower *Ccr7*, *Cd62l*, *Gpr183*, *Btla*, and *Slamf6* transcripts than FM Tfh cells (Figure 2E). We next performed unsupervised dimensionality reduction on the 25 gene × 126 cell matrix by non-negative matrix factorization (NMF) (Brunet et al., 2004) to determine whether the gene-expression pattern clustered cells based on their microanatomical location. This analysis showed that the data decomposed most robustly and reproducibly into two clusters (rank $k = 2$), as reflected by the high cophenetic correlation coefficient of 0.9995 (Figure S4). Analysis of expression of the two identified metagenes across samples showed partitioning of cells based on their location (Figures 2F and 2G). There was little difference between the original ordering (based on location) and re-ordered samples (based on metagene expression), suggesting that primary FM and GC Tfh cells are molecularly distinct and can be defined by expression of metagene P1 or P2, respectively. Accordingly, when samples are plotted by metagene expression, it is clear that GC Tfh cells are clustered together based on their high expression of metagene P2 and low expression of metagene P1, and FM Tfh cells based on their high expression of metagene P1 and low expression of metagene P2 (Figure 2G). The large Euclidean distance of 4.47 between the centroid of these clusters reflects their distinct molecular identity. Vector analysis showed that the major unique gene contributors to the metagene P2 (characteristic of GC Tfh cells) were *Bcl6*, *Pdcd1*, and *Il21*, and metagene P1 (characteristic of FM Tfh cells) were *Ccr7* and *Cd62l* (Figure 2H). Thus, primary GC Tfh cells have a distinct gene-expression signature from primary FM Tfh cells.

EBI2 Guides the Spatial Segregation of Primary Tfh Cells in the FM and GC

We noted from the single cell RT-qPCR that expression of *Gpr183*, the gene encoding EBI2, was downregulated in primary GC Tfh cells (Figure 2E) and therefore determined its surface

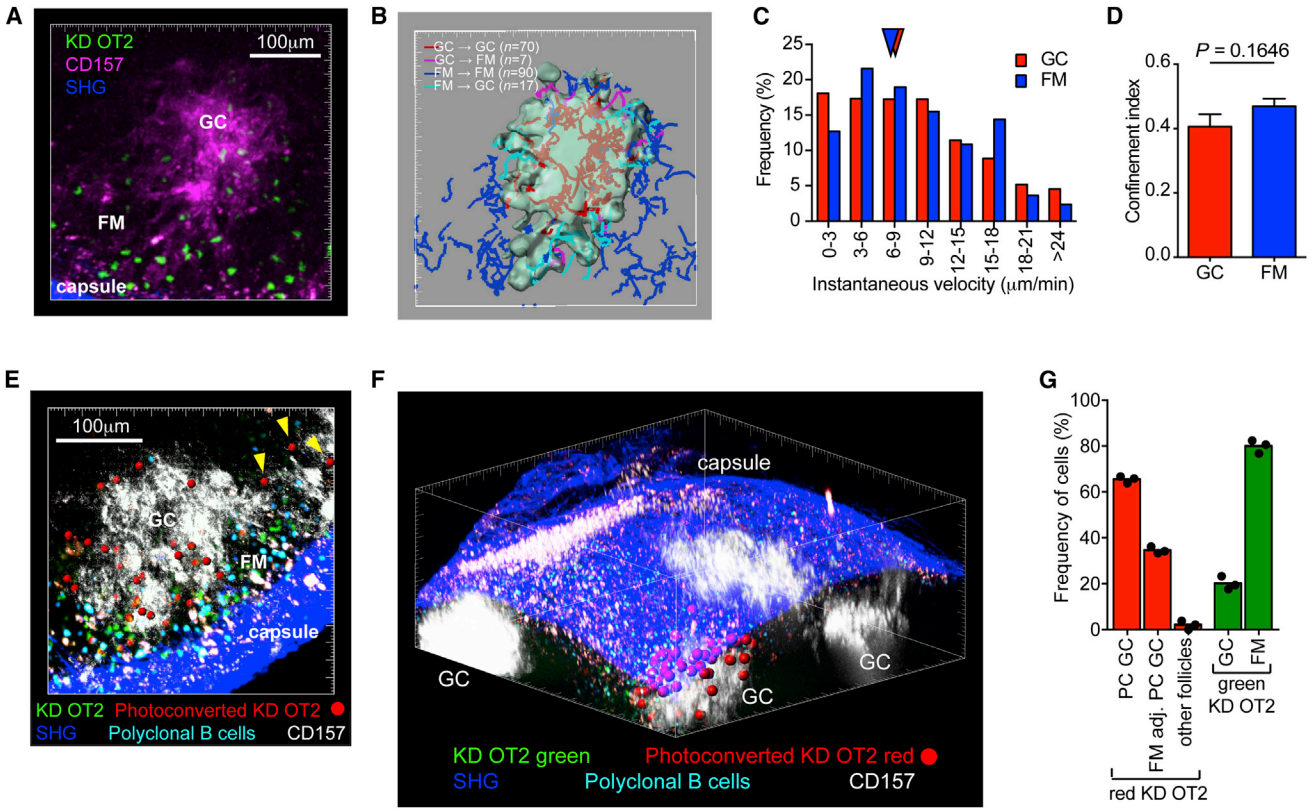

Figure 1. Spatial Segregation of Primary Tfh Cells into FM and GC Compartments

(A) Maximal intensity projection (398 × 390 × 75 μm) of follicle on day 7 showing primary Tfh cells (green) localize in the GC (magenta) and FM. Capsule is blue from SHG.

(B) Cell tracking analysis of (A) showing the spatial confinement of cells in the GC and FM. See also Movie S1.

(C) Distribution of instantaneous velocities of primary FM and GC Tfh cells. Arrows indicate median (7.8 μm/min for GC, and 8.5 μm/min for FM Tfh cells).

(D) Confinement index of primary GC and FM Tfh cells. Error bars indicate SEM.

(E) Retention of photoconverted GC Tfh cells (marked by red spheres) in the original follicle and GC (white) after 24 hr. Unphotoconverted Tfh cells are green; polyclonal B cells cyan and capsule blue from SHG. Yellow triangles indicate photoconverted cells that have migrated to the neighboring GC. See also Movie S2. Error bars indicate SEM.

(F) Cropped 3D rendered volume of lymph node from (E) showing confinement of photoconverted red cells (marked by red spheres) to the GC and FM of the original follicle.

(G) Comparison of the localization of photoconverted GC Tfh cells to unphotoconverted Tfh cells. PC GC, cells in photoconverted GC; FM adj. to PC GC, cells in FM adjacent to the original PC GC; other follicle, cells that have migrated outside follicle containing PC GC. Representative data (A–C, E and F) and pooled data (D and G) are from at least three experiments.

expression by Tfh cells as the immune response progressed (Figures 3A–3C). EBI2 was initially induced in antigen-specific KD OT2 cells, especially the $CXCR5^+PD\text{-}1^+$ cells, compared to endogenous $CD4^+$ T cells 3 days after immunization with OVA. It was then downmodulated on day 7 to be expressed in similar amounts on KD OT2 as endogenous $CD4^+$ T cells. On day 14, when most Tfh cells were localized in the GC and few remained outside in the FM, EBI2 was further downregulated in the $CXCR5^+PD\text{-}1^+$ subset. Thus, a clear subpopulation of $EBI2^{lo}$ Tfh cells could be detected by day 14 of the primary response (Figure 3C). We next optically marked FM and GC Tfh cells on day 7 and analyzed them by FACS (Figure 3D). This showed that EBI2 was specifically downregulated by a subset of GC Tfh cells that expressed the highest amount of PD-1. To test the role of EBI2 in primary Tfh cell localization, we retrovirally transduced OT2 T cells with either an empty or EBI2 expression vector (Figures 3E and 3F). Transduced cells expressing GFP were FACS sorted and adoptively transferred into wild-type recipients that were immunized with OVA. When draining lymph nodes were imaged on day 7, EBI2 overexpressing cells preferentially localized to the subcapsular and interfollicular region, and there was a nearly 2-fold reduction in the proportion of transduced OT2 Tfh cells in the GC. Conversely, EBI2-deficient KD OT2 T cell were 2.5-fold more efficient than wild-type KD OT2 T cells in localizing to the GC (Figures 3G and 3H). Thus, EBI2 provides one of the molecular cues needed to guide primary Tfh cells as they navigate between the GC and FM.

Follicular Memory T Cells Patrol the Outer Follicle and Scan SCS Macrophages for Antigen

We next tracked KD OT2 T cells after resolution of the immune response when the majority of GCs have collapsed. At these late time points, while the numbers of KD OT2 T cells have massively contracted, rare cells (20–200 per lymph node) were

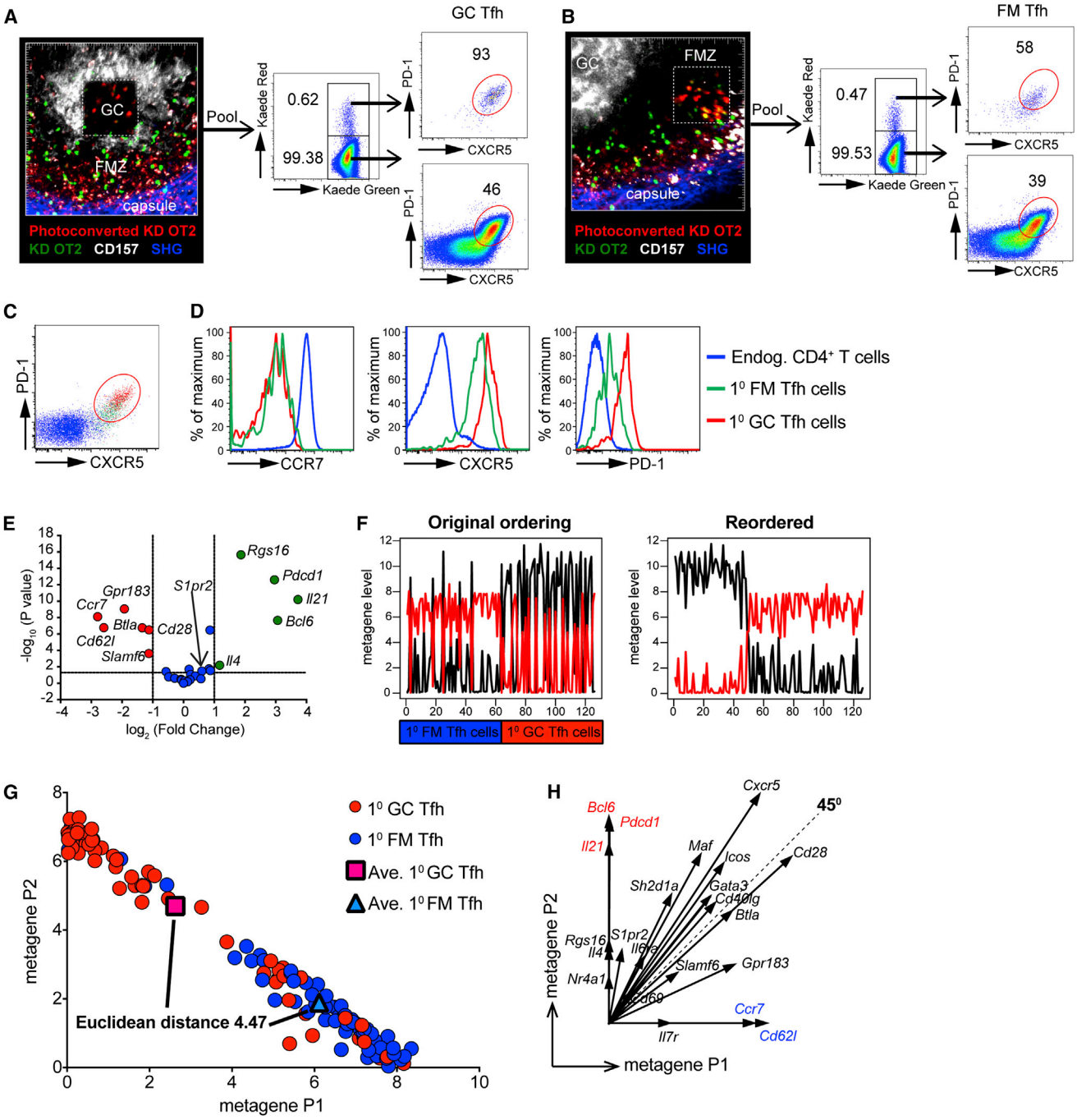

Figure 2. Primary FM and GC Tfh Cells Are Distinct Cell Populations

(A) Maximal intensity projection (332 × 332 × 99 μm) of follicle immediately after TPP of GC Tfh cells on day 7. Dashed box indicates the targeted ROI in the GC (white); unphotoconverted KD OT2 cells (green); photoconverted KD OT2 (red); capsule SHG (blue). Note bleaching of the GC label from photoconversion. Multiple lymph nodes were photoconverted and pooled. FACS analysis shows expression of CXCR5 and PD-1 by photoconverted red KD OT2 and unphotoconverted green KD OT2 cells.

(B) Maximal intensity projection (332 × 332 × 99 μm) of follicle immediately after TPP of FM Tfh cells. Fluorescent labels same as in (A). Multiple lymph nodes were photoconverted and pooled. FACS analysis shows expression of CXCR5 and PD-1 by photoconverted red KD OT2 and unphotoconverted green KD OT2 cells.

(C) FACS data from (A) and (B) were overlaid to show overlapping expression of CXCR5 and PD-1 by endogenous (blue), FM (green), and GC Tfh cells (red).

(D) Histograms of CCR7, CXCR5, and PD-1 expression by endogenous (blue), FM (green), and GC Tfh cells (red). Representative data from three experiments. KD OT2 cells in the FM (n = 62) and GC (n = 64) were optically marked by TPP and red cells FACS sorted for single cell RT-qPCR on day 7.

(E) Volcano plot showing differentially expressed genes in primary FM compared to GC Tfh cells. Downregulated genes are red, upregulated genes green, and non-differentially expressed genes blue. Intersecting lines indicate p-value of 0.05 and fold-change of 2.

(legend continued on next page)

still detectable by FACS analysis (see panel on day 28, Figure S5). Although the majority of these cells were CCR7$^+$ consistent with a central memory phenotype, a small subpopulation were CXCR5$^+$. We therefore injected anti-CD157 mAb the day before imaging to label the B cell follicle and scanned lymph nodes from immune animals to determine the location of these persistent cells (Figure 4A and Movie S3). These analyses showed that long-lived KD OT2 T cells could still be detected inside follicles following resolution of GCs where they comprised 20% of the memory cell pool. In vivo labeling of subcapsular sinus (SCS) macrophages with CD169 showed that the majority of the KD OT2 cells were located peripherally in the follicle and interfollicular regions (Figure 4B and Movies S3). This was confirmed by imaging from both the cortical and medullary side to depths of 360 μm (data not shown). Time-lapse two-photon microscopy showed these antigen-specific CD4$^+$ T cells persisting inside the follicle spent most of their time (>75%) in close proximity to SCS macrophages where they migrated with significantly reduced instantaneous velocity, increased arrest coefficient and reduced motility coefficient compared to when they were deeper in the follicle, consistent with antigen surveillance (Figures 4C–4G and Movie S4). These cells were observed to make extensive surface contacts with SCS macrophages as demonstrated by colocalization analysis (Figure 4H and Movie S4). Unfortunately, the rarity of these cells and degradation of photoconverted Kaede protein after several weeks (Chtanova et al., 2014) presented major technical challenges to their phenotypic characterization and lineage tracing. Nevertheless, we have used the term ''follicular memory T cell'' purely to denote their location inside the follicle (in contrast to the extrafollicular memory T cells) without making any assumptions about their origin or relationship to Tfh cells.

Follicular Memory T Cells Are Activated in the Subcapsular Region upon Antigen Recall

Given the localization of these memory T cells in the outer follicle, we next asked whether this was also the site of secondary Tfh cell activation. Initially, we used OVA-PE to show that antigen, possibly bound in immune complexes by neutralizing anti-OVA antibodies generated from the initial immunization, is rapidly transported to the lymph node upon rechallenge where it is captured and displayed by CD169$^+$ macrophages lining the SCS and interfollicular zones within 4 hr (Figures 5A and 5B). By comparison, there was less capture of the irrelevant antigen hen egg lysozyme (HEL)-PE (to which there were no immune antibodies) in the subcapsular region (Figures 5A and 5B). Even in this short time period, there was increased accumulation of lymph node resident memory T cells in the subcapsular region in response to the cognate antigen OVA-PE (98% of cells in the follicle) but not HEL-PE (74% of cells, similar to the ''resting'' follicular memory T cells see Figure 4D) (Figure 5C). Time-lapse two-photon microscopy of draining lymph nodes 2 days after rechallenge with OVA showed secondary Tfh cells slowed down and stopped migrating when they came into contact with SCS macrophages (Figure 5D), in contrast to the active scanning by ''resting'' follicular memory T cells before antigen recall (Figure 4H). Accordingly, secondary Tfh cells in the subcapsular region had a rounded morphology and higher arrest coefficient than those in the inner follicle (Figures 5E–5G and Movie S5) suggestive of TCR engagement. We also observed memory T cells undergoing cell division while in contact with SCS macrophages (Figure 5H and Movie S5). Thus, the secondary immune response in the lymph node is initiated in the subcapsular region.

Migration of Secondary Tfh Cells out of the GC and Lymph Node Is Unrestricted

We next determined the migration pattern and behavior of secondary Tfh cells (Figures 6A–6D). Upon antigen recall, a more rapid GC response is generated that peaks on day 5, two days earlier than in the primary response (Figure S5). The Tfh cell response to secondary antigen is stereotyped by rapid generation of an almost uniform population of CXCR5$^+$CCR7^{lo}PD-1^{hi} cells. Secondary Tfh cells were seen to migrate from the GC to the FM at a 5-fold higher frequency than in the primary response (7/77 GC tracks going from GC to FM in Figure 1B compared to 7/15 in Figure 6B, see also Movies S1 with S6). However, secondary Tfh cells located in the GC and FM had similar motility parameters (Figures 6C and 6D). Activated memory KD OT2 T cells were observed to crawl between the cells lining the floor of the SCS to enter the lumen where they became rounded and to detach and be carried away in the lymphatic flow (Figures 6E and 6F, and Movie S7). We also observed activated memory KD OT2 cells arriving in the follicle via the lymphatics, presumably from an ''upstream'' follicle. In fact, when we optically marked secondary Tfh cells in the GC and reimaged the next day, >97% of the photoconverted cells had left the GC and relocalized to the FM in the original photoconverted follicle or migrated to the FM of neighboring and distant follicles (Figures 6G and 6H and Movie S7). These data contrast with the migration pattern of primary Tfh cells (Figures 1A and 1B and Movie S1). Thus, Tfh cells in the secondary response are not confined to the GC and instead are able to migrate in and out of the follicle via the SCS.

Secondary Tfh Cells in the FM and GC Are Molecularly Heterogeneous

To investigate the differences in the migratory behavior between primary and secondary Tfh cells, we first examined surface expression of CCR7 and CXCR5 by optically marked cells in the FM and GC (Figure 7A). These analyses showed that unlike the primary response, secondary Tfh cells expressed similar amounts of these chemokine receptors irrespective of their microanatomical compartment of origin. Both groups of secondary Tfh cells expressed high amounts of *Bcl6* (Figure 7B). However, there were changes in the expression pattern of *Ccr7*, *Cxcr5*, *Gpr183*, and *S1pr2* (Figure 7C). In particular, differences in expression that arose in the primary response were abolished

(F) Expression profile of two metagenes identified by NMF analysis across primary FM and GC Tfh cells (left panel), and across the samples re-ordered according to relative metagene expression (right panel). Red, metagene P1; blue, metagene P2.
(G) Cluster analysis of primary FM and GC Tfh cells. Metagene P2 expression was plotted against metagene P1 expression for each cell.
(H) Vector loadings of each gene to metagene P1 and P2. Single cell expression data is pooled from two identical independent experiments.

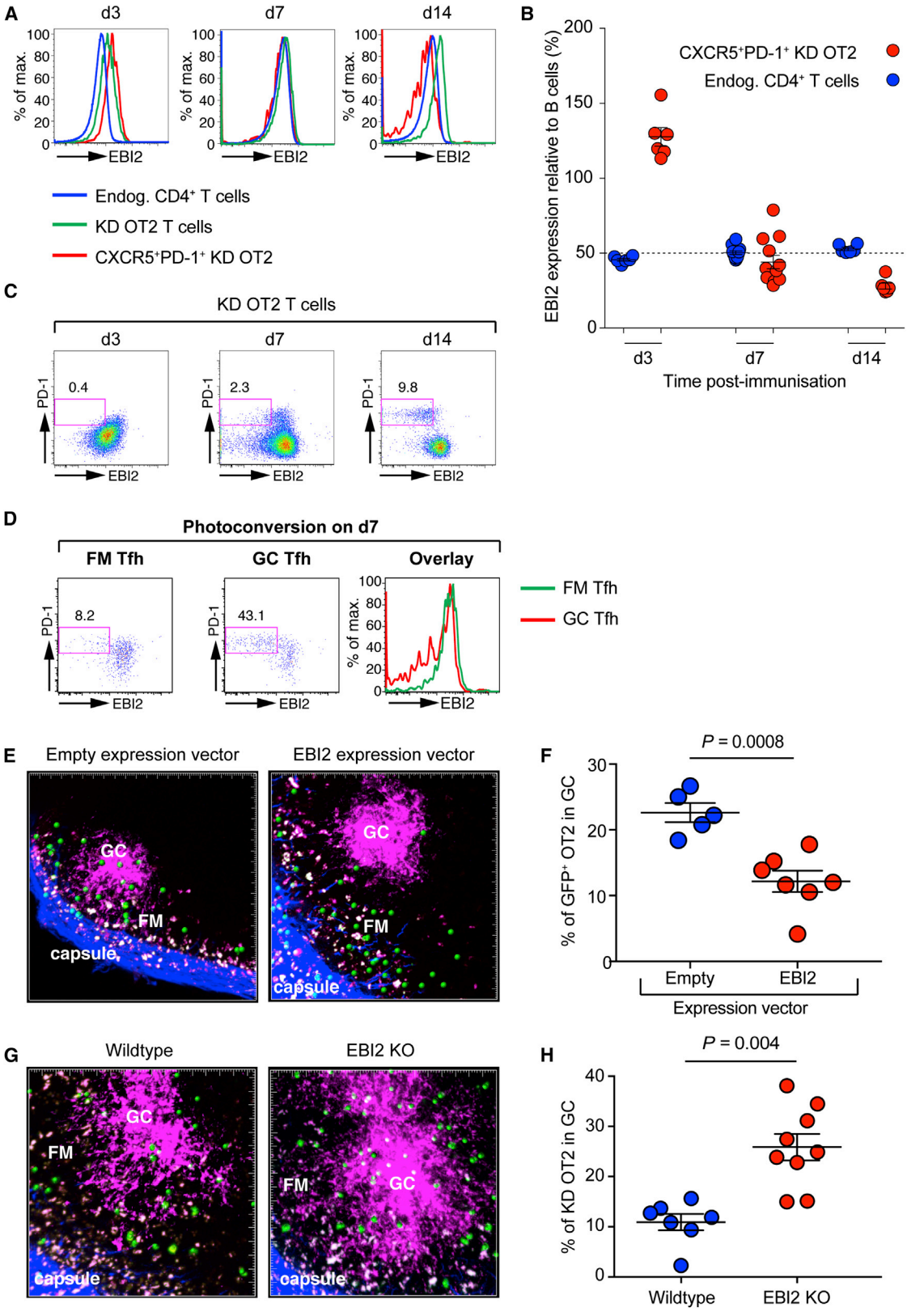

(legend on next page)

in secondary Tfh cells. For example, selective downmodulation of *Gpr183* by primary GC Tfh was not observed in secondary the response where both FM and GC Tfh cells maintained high expression of this gene. This suggests that EBI2 was not involved in GC positioning of secondary Tfh cells and, consistent with this, EBI2-deficient KD OT2 T cells were able to generate secondary Tfh cells and colonize the GC upon rechallenge with the same efficiency as wild-type B cells (data not shown). Furthermore, selective induction of the regulator of G protein signaling family member *Rgs16* (Estes et al., 2004) in primary GC Tfh cells was also absent in the secondary response (Figure 7D). These data suggest that the differences in migratory behavior of Tfh cells in the primary and secondary response result from loss of differential chemokine receptor expression and sensitivity to global positioning signals by secondary Tfh cells in the GC and FM.

The free exchange of secondary Tfh cells between the FM and GC raised the possibility that, unlike the situation in the primary response, these are no longer molecularly distinct cell populations. This was also suggested by their similar gene-expression profiles (Figure 7E). To explore this further, we analyzed the 25 gene × 126 cell matrix from secondary Tfh cells by NMF and found that while the data could be stably decomposed into two clusters (k = 2, cophenetic correlation coefficient = 0.9654, Figure S6), these clusters did not segregate according to microanatomical location (Figure 7F). Indeed, the existence of the two factorized subpopulations was only apparent after reorganization of the cells based on their metagene expression (Figure 7G). Thus, individual secondary Tfh cells from the FM and GC overlap in expression of metagenes S1 and S2 and were only separated by a Euclidean distance of 0.04 (Figure 7H). Vector analysis showed the major unique contributors to metagene S2 were *Bcl6* and *Pdcd1* (Figure 7I). Therefore, NMF analysis points to the presence of two molecular subpopulations that exist heterogeneously within both the FM and GC, rather than a homogeneous secondary Tfh cell population as would be inferred from the FACS (Figure 7A) and volcano plot (Figure 7C). Finally, we also combined the single cell gene expression data from primary and secondary responses and performed NMF analysis on all four groups (Figure S7). This confirmed the previous analyses and reproducibly identified primary GC Tfh cells as being molecularly distinct from secondary Tfh and primary FM Tfh cells. In addition, secondary Tfh cells from the FM and GC could not be resolved from each other even when model conditions were relaxed to allow for multiple clusters (rank k = 2–5).

DISCUSSION

The origin and fate of Tfh cells has been intensely studied since their first description 14 years ago (Breitfeld et al., 2000; Schaerli et al., 2000). Although mice engineered to report BCL6 (Kitano et al., 2011; Liu et al., 2012) and interleukin-21 (IL-21) (Lüthje et al., 2012) expression have provided powerful tools to analyze Tfh cells, their usefulness has been limited by Tfh cell heterogeneity and plasticity (Cannons et al., 2013). In this regard, the development of methods for the optical marking and tracking of cells based on their microanatomical location have created further opportunities for more precise delineation of Tfh cell dynamics and the molecular cues that underpin their behavior. Here we have used optical marking by TPP to link Tfh cell location to their behavior, phenotype, and gene expression. Our studies show remarkable differences in the migration pattern and single cell gene-expression signatures between primary and secondary Tfh cells. In addition, we report a subpopulation of "follicular memory T cells" that reside in the follicle where they scan SCS macrophages to initiate the secondary immune response upon antigen re-exposure. This temporospatial dissection of Tfh cell dynamics offers multiple new insights into regulation of GC responses in naive and antigen-experienced animals.

Imaging of primary Tfh cells at the peak of the GC response revealed clear spatial segregation in the FM and GC compartments. This confinement was confirmed by TPP and discontinuous cell tracking 24 hr later, which showed retention of the majority of photoconverted GC Tfh cells in the original GC and follicle. Furthermore, NMF analysis of single cell gene expression signatures of FM and GC Tfh cells support the notion that they represent molecularly distinct cell populations. Thus, we conclude that the primary GC is a closed structure designed to partition responding GC B cells and restrict their access to $CD4^+$ T cell help. At face value, these data contrasts with the findings of Shulman et al. who concluded that the GC is an open structure designed to broaden the diversity of the available $CD4^+$ T cell help (Shulman et al., 2013). However, the preliminary experiments in their paper only examined polychromatic responses in naive animals that demonstrated initial colonization by multiple clones of red, green, or cyan T cells with the same TCR specificity and not interfollicular exchange as claimed. Furthermore, their subsequent experiments involved prime-boost immunization protocols that involved repeated exposure to antigen. This is a critical point of difference as they do not show any equivalent photoactivation data from naive responses

Figure 3. EBI2 Promotes the Spatial Segregation of Primary FM and GC Tfh Cells

(A) Overlay histogram from FACS analysis for EBI2 expression by endogenous $CD4^+$ (blue), KD OT2 (green) and $CXCR5^{hi}PD\text{-}1^+$ KD OT2 T cells (red) on day 3, 7 and 14.

(B) Plot of EBI2 expression relative to $B220^+$ B cells by endogenous $CD4^+$ (blue) and $CXCR5^{hi}PD\text{-}1^+$ KD OT2 T cells (red) from (A). (C) FACS plot of EBI2 and PD-1 expression by KD OT2 T cells from (A).

(D) EBI2 expression by optically marked FM and GC Tfh cells on day 7.

(E) Localization OT2 T cells retrovirally transduced with either empty (left panel) or EBI2 (right panel) expression vector on day 7 after GFP^+ cells were sorted, adoptively transferred, and immunized.

(F) Quantification of the proportion of green Tfh cells that localize to the GC from (E). Error bars indicate SEM.

(G) Localization of KD OT2 cells from wild-type (left panel) and EBI2-deficient (right panel) donors on day 7 after adoptive transfer and immunization. Error bars indicate SEM.

(H) Quantification of the proportion of green Tfh cells that localize to the GC from (G). Representative data (A, C, D, E, and G) and pooled data (B, F, and H) from three independent experiments are shown.

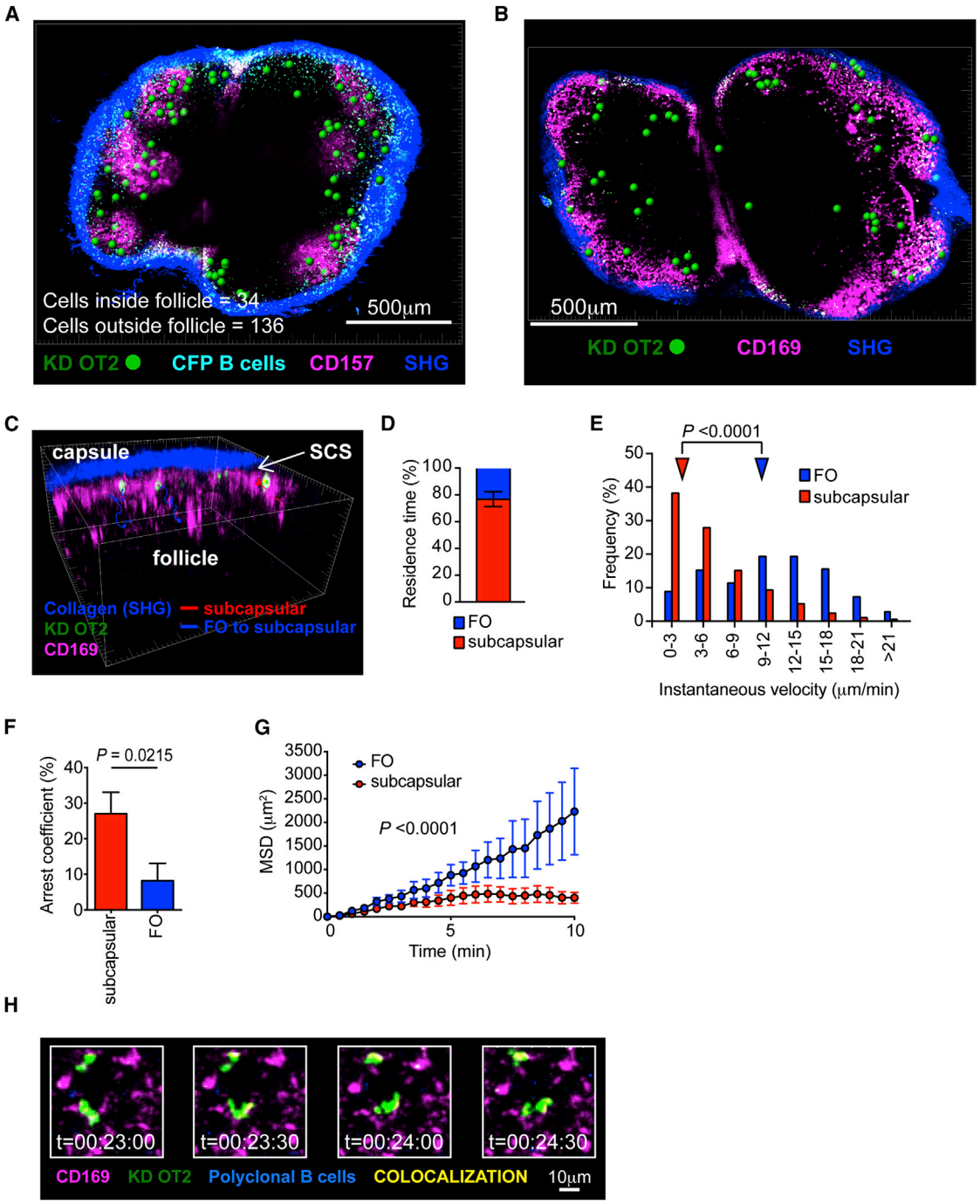

Figure 4. Follicular Memory T Cells Localize to the Outer Follicle and Scan SCS Macrophages

(A) Maximal intensity projection (1992 × 1494 × 30 μm) of immune lymph node on day 35 showing persistence of antigen-specific KD OT2 T cells (marked by green spheres) in the follicle (magenta). Collagen in capsule is blue, polyclonal CFP B cells are cyan. The number of cells inside and outside follicles for the whole tiled volume is shown. See also Movie S3.

(B) Maximal intensity projection (2124 × 1274 × 30 μm) of immune lymph node on day 30 showing persistence of antigen-specific KD OT2 T cells (marked by green spheres) in the proximity to CD169$^+$ SCS macrophages (magenta). Collagen in capsule is blue. See also Movie S3.

(C) Rendered 212 × 212 × 99 μm volume of draining lymph node 37 days after primary immunization. Follicular memory T cells (green) localize in the periphery adjacent to SCS macrophages (CD169, magenta). Tracks of follicular memory T cells scanning SCS macrophages (red line) and migrating from the follicle up to the SCS macrophages (blue lines) are shown. See also Movie S4.

(D) Residence time of follicular memory T cells in the follicle and subcapsular region. Individual tracks were segmented based on their proximity to SCS macrophages and the residence time as percentage of track duration calculated.

(legend continued on next page)

(Shulman et al., 2013). Hence, their data is more consistent with our memory responses. In fact, we not only observed the migration of Tfh cells out of the GC in the secondary response but also their transport in the lymphatic flow of the SCS. This passive transport mechanism whereby cells "surf" the lymph appears to be an efficient and rapid mechanism for dissemination of cells that bypasses the need to traverse multiple anatomical compartments across disparate chemokine gradients. Regardless, it will be interesting to determine what role factors enriched in lymph, such as S1P, play in driving secondary Tfh cells to enter and leave the follicle.

Why are Tfh cell dynamics so fundamentally different in naive and immune animals? Initially, GC B cells must pass stringent affinity and specificity checkpoints to ensure only high-affinity non-self-reactive cells are selected. Therefore, restricting primary Tfh cells with the greatest helper capacity to the GC might serve to direct help to cognate B cells and avoid the activation of bystander B cells in the follicle. Accordingly, expression of the genes encoding the B helper cytokines IL-21 and IL-4 were restricted to primary GC Tfh cells. In the secondary response, memory B cells have already passed these checkpoints and therefore have less stringent activation thresholds. Correspondingly, secondary Tfh do not express the same high amounts of *Il21* and *Il4* transcripts as primary GC Tfh cells. Furthermore, memory B cells are widely distributed in persistent GC remnants within the follicle (Dogan et al., 2009; Talay et al., 2012) and extrafollicular sites including the bone marrow (Dogan et al., 2009; Paramithiotis and Cooper, 1997), tonsillar mucosal epithelium (Liu et al., 1995) and splenic marginal zone (Liu et al., 1988). Therefore, protective secondary antibody responses may depend on the rapid extrafollicular export of secondary Tfh cells to these sites. Thus, unlike primary responses where it takes 7 days or more for Tfh cells to mature, the stereotypic expansion of $CXCR5^{hi}PD\text{-}1^{hi}$ cell with a "mature" Tfh cell phenotype that peaks by day 3 in our system may be a part of a pre-wired memory program (Hale et al., 2013). Nevertheless, some memory B cells do enter GCs (Dogan et al., 2009; Pape et al., 2011) and Tfh cells are still required in this location in the secondary response. In this respect, it is notable that the NMF analysis of single cell gene expression by secondary Tfh cells showed that there was a hidden subpopulation of cells with high expression of *Bcl6* and *Pdcd1* that might be destined to later colonize and persist in secondary GCs. Thus, follicular memory T cells also appear to bifurcate into two responding populations upon rechallenge. However, at the peak of the secondary Tfh response these responding cells are equally likely to be in the FM or GC.

What are the molecular signals that guide Tfh cells as they navigate around the lymph node in the course of the immune response? It was recently reported that Tfh cells inside GCs have high expression of SIPR2, which acts to repel them from the S1P-rich lymph in the SCS and promote their retention in the GC (Moriyama et al., 2014). While *S1pr2* was also upregulated in our single cell gene-expression analysis by primary GC Tfh cells, there were more striking changes in *Gpr183* gene and EBI2 protein expression. Moreover, gene-function analysis using retroviral transduction and knockout mice confirmed a role for EBI2 in primary GC localization. These data also closely parallel the role of EBI2 in the positioning of GC B cells (Gatto et al., 2009; Pereira et al., 2009). Conspicuously, there was no differential expression of a number of chemokine receptors including *Cxcr5*, *Ccr7*, *S1pr2*, and *Gpr183* in secondary Tfh cells located in the FM and GC, and this may explain the lack of spatial confinement upon antigen recall. Accordingly, we did not detect a defect in GC localization by EBI2-deficient KD OT2 T cells in secondary responses. Furthermore, *Rgs16* was induced in primary, but not secondary, GC Tfh cells, suggesting an additional layer of control in chemokine receptor signaling allows the cells to integrate the changes in expression of these and possibly other chemokine receptors to determine their global positioning.

Our finding that follicular memory T cells are located in the periphery of the draining lymph node is reminiscent of the CXCR3-dependent positioning of memory $CD8^+$ T cells in this location (Kastenmüller et al., 2013). This positioning of follicular memory T cells at the lymph-tissue interface might facilitate quick and efficient surveillance of SCS macrophages which act as "fly paper" (Junt et al., 2007) to capture lymph-borne antigens (Carrasco and Batista, 2007; Junt et al., 2007; Phan et al., 2007; Roozendaal et al., 2009), particularly the antigen-antibody immune complexes that are generated upon secondary exposure (Phan et al., 2007; Roozendaal et al., 2009). While SCS macrophages are slow to phagocytose (Phan et al., 2009), they are nevertheless still capable of processing and presenting protein antigen to $CD8^+$ T cells (Chtanova et al., 2009; Hickman et al., 2008) and lipid antigens to iNKT cells (Barral et al., 2010). Thus, the finding that follicular memory T cells are activated to proliferate in the subcapsular region also resolves the question of where the secondary antibody response is initiated. Memory B cells were recently shown to induce rapid BCL6 upregulation by "memory Tfh cells" in the spleen in the absence of dendritic cells (Ise et al., 2014). However, these experiments examined recall responses in the spleen of naive recipient mice following adoptive transfer of FACS-sorted "memory Tfh cells." In contrast, we examined the in situ recall responses made by persistent antigen-specific cells in the lymph node of immune animals without any ex vivo manipulation. It should also be noted that other groups have been able to generate robust memory responses in naive recipient mice without the need for cotransfer of memory B cells (Lüthje et al., 2012; Weber et al., 2012). Hence, while memory B cells might support secondary Tfh responses at the T-B border under some circumstances, it is likely that local responses in draining lymph nodes can also be generated in the subcapsular region. Importantly, this

(E) Median instantaneous velocity of follicular memory T cells when in the follicle (11.3 μm/min) and in proximity to SCS macrophages (4.0 μm/min) were calculated from track segments.

(F) Arrest coefficient defined as percentage of time a cell slowed down to <3 μm/min. Error bars indicate SEM.

(G) Motility coefficients for cells while distal (blue) and proximal to SCS macrophages (red). Data is pooled from 42 track segments from 26 individual cells tracked in three separate mice. Error bars indicate SEM.

(H) Time-lapse images showing follicular memory T cells (green) scanning SCS macrophages (magenta) for antigen. Colocalization channel between green and magenta is pseudo-colored yellow. Time stamp is hh:mm:ss. See also Movie S4.

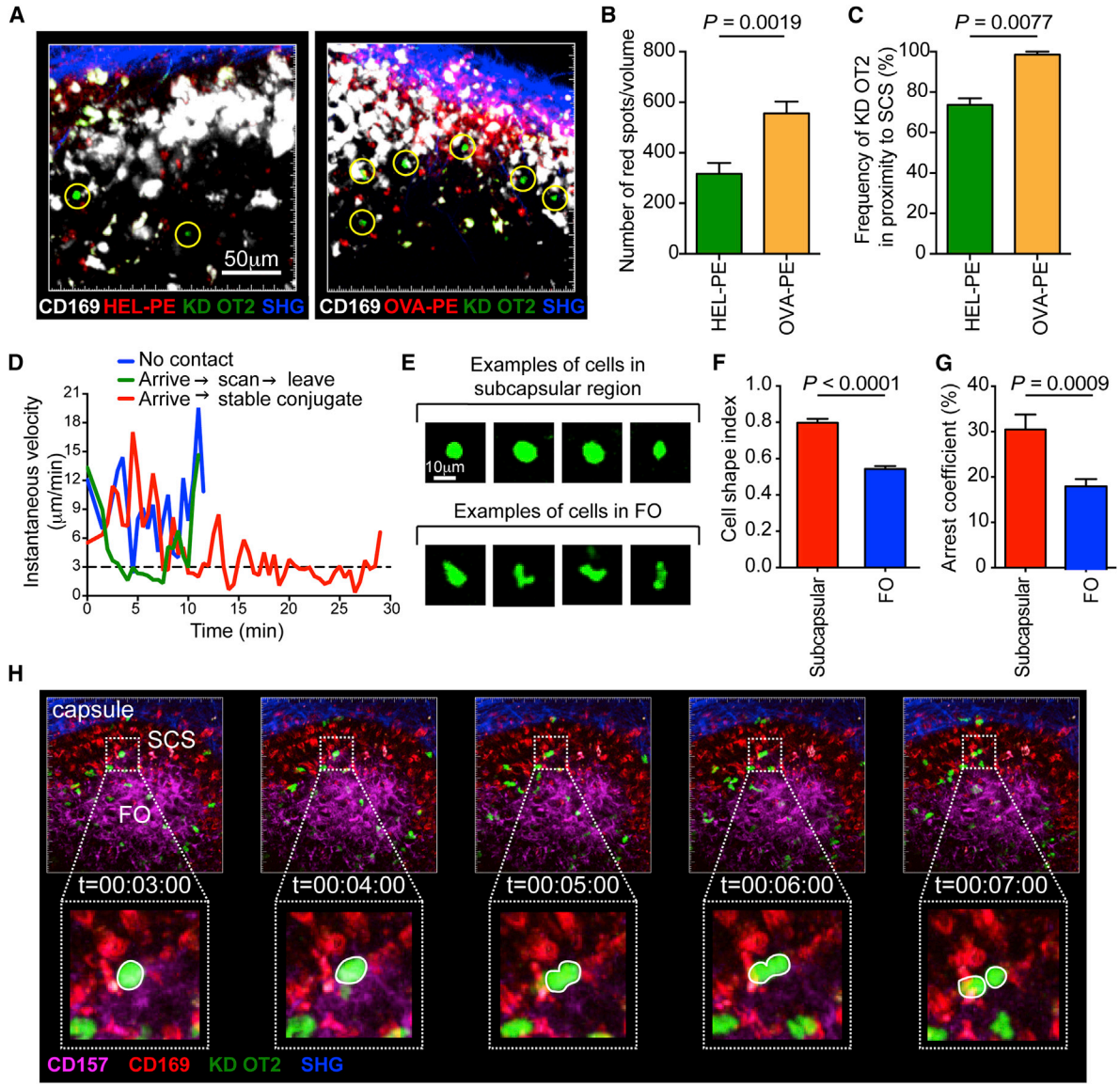

Figure 5. Follicular Memory T Cells Are Activated in the Subcapsular Region

(A) Comparison of antigen trapping of red HEL-PE control (left) and OVA-PE immune complexes (right) by SCS macrophages (white) 4 hr after injection. Note the follicular memory T cells (green highlighted with yellow circle).

(B) Quantification of amount of antigen trapping by counting red spots. Error bars indicate SEM.

(C) Redistribution of follicular memory T cells to the subcapsular region 4 hr after rechallenge with OVA-PE but not HEL-PE. Error bars indicate SEM.

(D) Examples of cells migrating on day 2 after rechallenge in relation to SCS macrophages.

(E) Mice were rechallenged with OVA and draining lymph node imaged 2 days later. Still frames show representative secondary Tfh cells in the subcapsular region (top) and inner follicle (bottom). See also Movie S5.

(F) Cell shape index calculated for 56 cells in the subcapsular region and 98 cells in the inner follicle.

(G) Arrest coefficient calculated for 67 cell tracks in the subcapsular region and 197 cell tracks in the inner follicle. Error bars indicate SEM.

(H) Selected time-lapse images on day 2 after rechallenge showing a secondary Tfh cells dividing (white outline, inset) in contact with CD169-labeled SCS macrophages (red). Follicular stroma (magenta); capsule SHG (blue). See also Movie S5.

temporospatial organization of memory responses bypasses the need for shuttling of primary Tfh cells from the T cell zone to the T-B border and finally into the follicle, and ensures rapid intrafollicular generation of secondary Tfh cells. Taken together, these data show that Tfh cell heterogeneity and complexity can be resolved by temporospatial dissection of their behavior and the molecular cues that guide this behavior. It is hoped that future studies using non-linear optical marking and single cell genomics will reveal further insights into Tfh cell biology and thereby provide cellular and molecular targets that could be manipulated to augment or dampen the antibody response to treat human diseases.

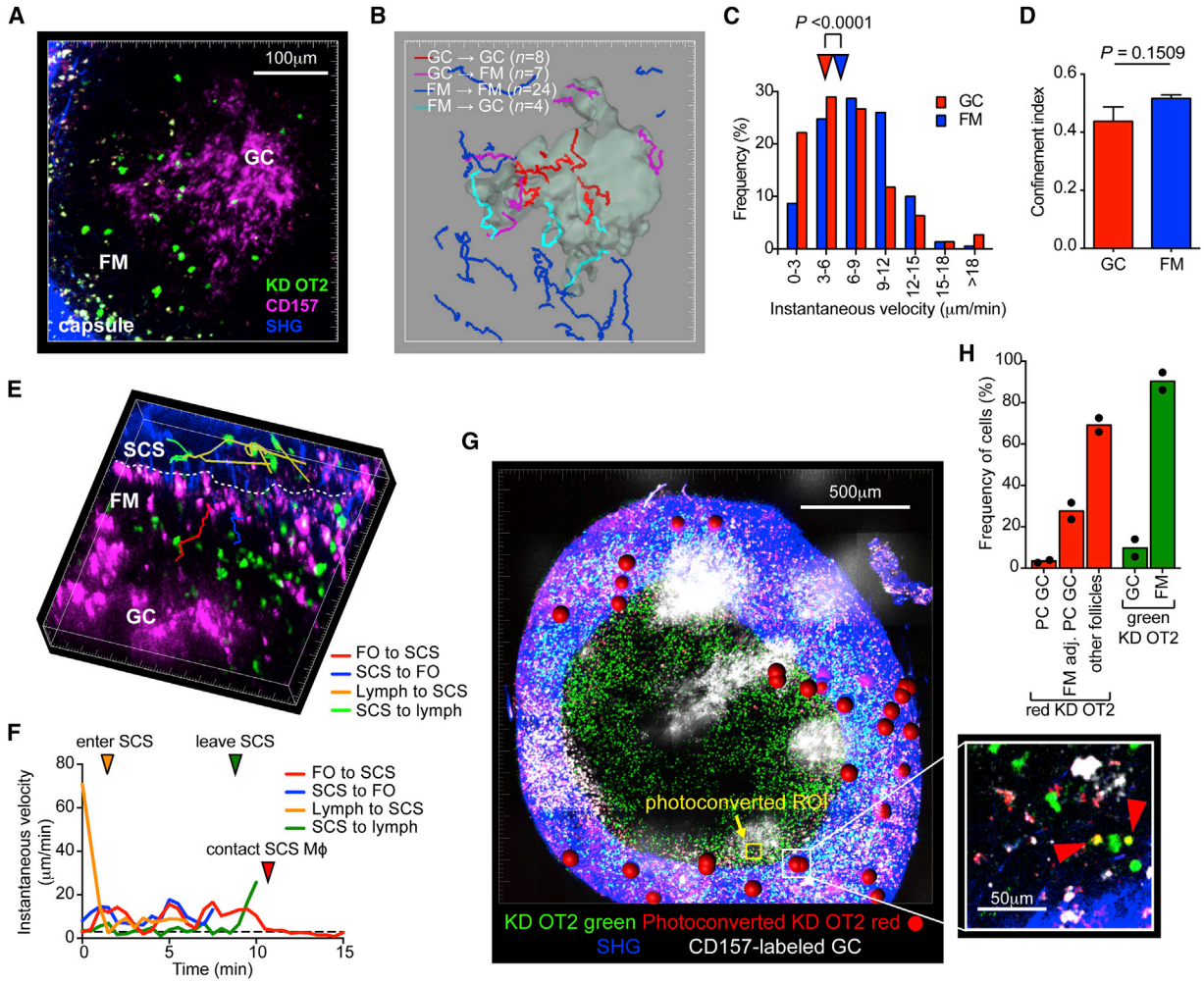

Figure 6. Secondary Tfh Cells Enter and Leave the Follicle via the Lymphatics

(A) Maximal intensity projection (393 × 407 × 96 μm) of follicle on day 5 after rechallenge showing secondary Tfh cells (green) localize in the GC (magenta) and FM. Capsule is blue from SHG.

(B) Cell tracking analysis of (A) showing the spatial confinement of cells in the GC and FM. See also Movie S6.

(C) Distribution of instantaneous velocities of secondary Tfh cells in the FM and GC. Arrows indicate median (5.8 μm/min for GC and 7.6 μm/min for FM).

(D) Confinement index of secondary Tfh cells in the FM and GC. Error bars indicate SEM.

(E) Rendered 332 × 332 × 51μm volume showing secondary Tfh cells (green) entering (yellow tracks) and leaving the follicle (green tracks) via the SCS. Tracks of secondary Tfh cells migrating from the follicle to subcapsular region (red) and from the subcapsular region to the follicle (blue) are shown for comparison. See also Movie S7.

(F) Instantaneous velocities of representative tracks from (E) showing changes in relation to their microanatomical location. Dashed line indicates threshold of 3 μm/min.

(G) Cropped mosaic tile image of lymph node showing dissemination of photoconverted GC Tfh cells (marked by red spheres) out of the original follicle after 24 hr. Unphotoconverted Tfh cells, green; polyclonal B cells, cyan; capsule, blue from SHG. Inset shows raw image from single optical plane with two photoconverted cells (yellow; red arrows) located just beneath the capsule. See also Movie S7.

(H) Comparison of the GC localization of photoconverted to unphotoconverted secondary Tfh cells. PC GC, cells in photoconverted GC; FM adj. to PC GC, cells in FM adjacent to the original PC GC; other follicle, cells that have migrated outside follicle containing PC GC. Data is from at least three experiments.

EXPERIMENTAL PROCEDURES

Animals and Immunizations

Transgenic and knockout mice used are described in Supplemental Experimental Procedures. For primary responses, 2.5 × 10^5 $CD4^+V_a2^+$ KD OT2 cells were adoptively transferred into age and sex-matched 6- to 10-week-old SAP-deficient recipient mice and immunized with 20 μg of OVA in Sigma Adjuvant System (SAS, Sigma). For memory responses, immunized mice were rested for 28–95 days and rechallenged with 40 μg of OVA in SAS. In some experiments, we also co-transferred 2.5 × 10^5 HEL^+ SW_{HEL} tdTomato B cells and V_a2^+ $CD4^+$ KD OT2 into SAP-deficient recipients and immunized with 20 μg HEL-OVA. To label the GC in vivo, we injected anti-CD157 subcutaneously 3-4 days before imaging. See Figure S3 and Supplemental Experimental Procedure for detailed description and validation of this labeling strategy.

Retroviral Transduction of Primary T Cells

$CD4^+$ OT2 T cells were stimulated with peptide-pulsed irradiated splenocytes and retrovirally transduced with gene encoding EBI2 or empty cassette (Gatto

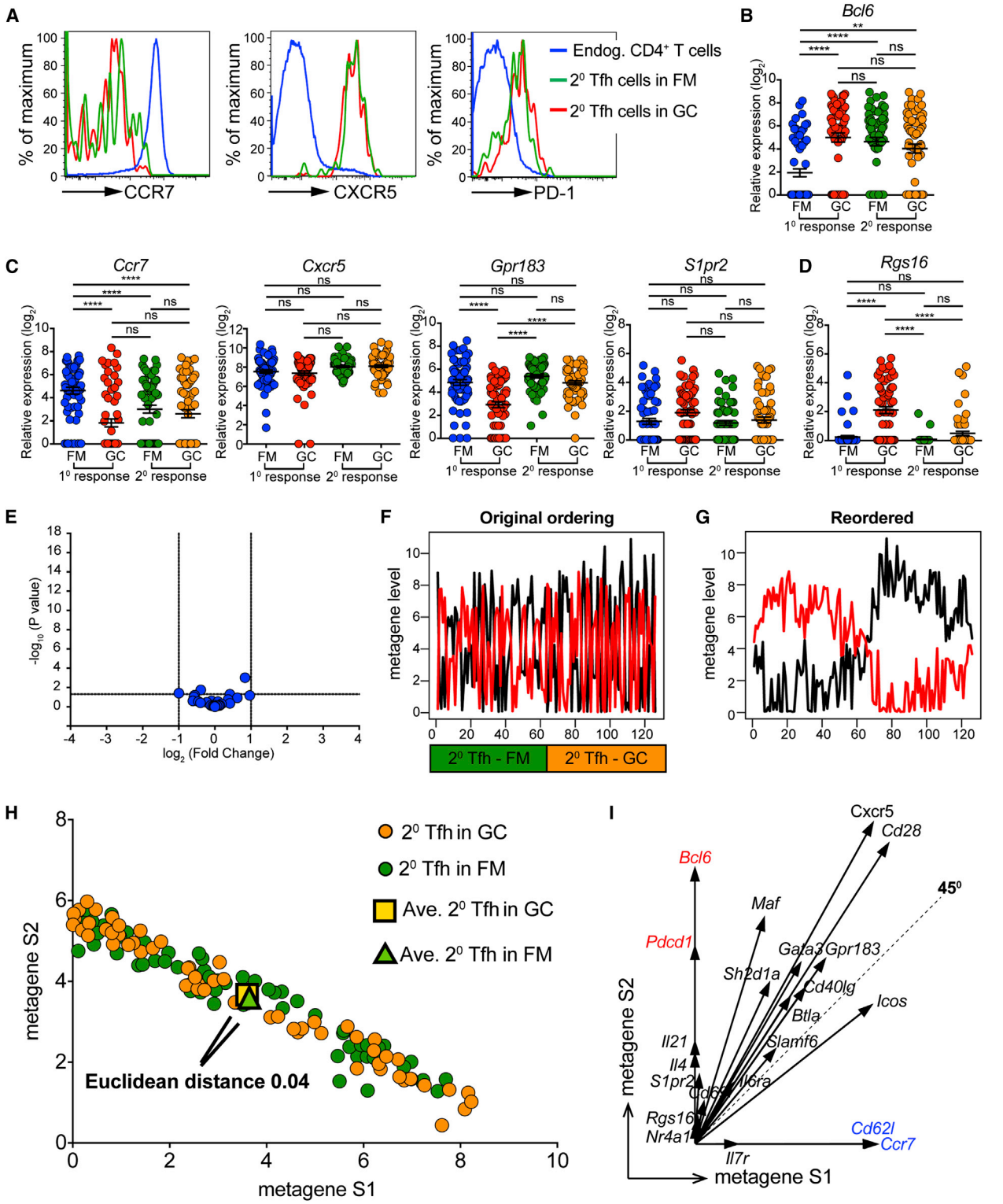

Figure 7. Secondary Tfh Cells from FM and GC Share the Same Phenotype and Gene Expression Patterns

Recipient mice were immunized and re-challenged 30 days later. Lymph nodes were harvested at the peak of the secondary response on day 5 post antigen-recall and cells in the FM and GC photoconverted for FACS analysis and single cell RT-qPCR.

(A) Histograms of CCR7, CXCR5, and PD-1 expression by endogenous (blue), FM (green), and GC Tfh cells (red) from the secondary response. Representative data from two independent experiments. Relative single cell expression of (B) *Bcl6*, (C) *Ccr7*, *Cxcr5*, *Gpr183*, and *S1pr2*, and (D) *Rgs16*. Error bars indicate SEM.

(E) Volcano plot comparing expression of 25 genes by secondary Tfh cells in the FM (n = 64) and GC (n = 64).

(legend continued on next page)

et al., 2009). FACS-sorted CD4$^+$V$_\alpha$2 TCR$^+$eGFP$^+$ retrovirally transduced cells were then adoptively transferred and recipient mice immunized 6 hr later. Draining inguinal lymph nodes were analyzed by two-photon microscopy to determine the localization of transduced cells on day 7. See also Supplemental Experimental Procedures.

Two-Photon Microscopy and Two-Photon Photoconversion

Intravital two-photon microscopy and TPP was performed as previously described with some minor changes (Chtanova et al., 2014). Briefly, mice were anesthetized and kept warm on a custom heated SmartStage (Biotherm) set to 38°C. The inguinal lymph node was mobilized along with the intact inguinal ligament in a skin flap and and the cortical surface of the lymph node was exposed by microdissecting the skin and overlying fat and fascia layers. Imaging was performed on a Zeiss 7MP two-photon microscope (Carl Zeiss) powered by a Chameleon Vision II ultrafast Ti-Sa laser (Coherent Scientific). TPP was achieved by real-time interactive scanning of ROIs with 840 nm NIR excitation laser pulses for 2,000–5,000 cycles at varying laser power intensities to achieve optimal photoconversion as determined by loss of green and acquisition of red signal (Chtanova et al., 2014). TPP was non-toxic as demonstrated by the fact that cells within the photoconversion volume continued to migrate with the same velocities before, during, and after TPP.

Image Analysis and Cell Tracking

Cells were detected using the spot detection function in Imaris (Bitplane) and the automatically generated tracks were manually verified. Motility parameters were extracted from the Imaris Statistics function. In some experiments, surfaces were applied to delineate the boundaries of GCs using the Imaris Surface function. For these analyses, the GC was defined as the CD157-rich center of the follicle and the FM was defined as the surrounding CD157-negative area between the GC and capsule. For analysis of cell behavior when distant (>20 μm) and proximal (<20 μm) to SCS macrophages, individual tracks were manually checked at each time point to determine their position in relation to the CD169$^+$ SCS macrophages.

FACS Analysis and Single Cell FACS Sorting

FACS analysis was performed as described (Phan et al., 2009). Single cell FACS sorting was performed into a 96-well skirted PCR plate on a FACS Aria II as described (Phan et al., 2005). See also Supplemental Experimental Procedures.

Single Cell RT-qPCR

RNA was isolated from single FACS sorted cells using the Ambion Single Cell to CT kit (Life Technologies) according to the manufacturer's instructions. See also Supplemental Experimental Procedures.

Gene Expression Analysis by NMF

Gene-expression analyses were carried out on a complete log-transformed normalized dataset of 32 genes across 252 single-cell samples (8064 transcripts). Seven genes (*Foxp3*, *Ifng*, *Il2ra*, *Prdm1*, *Rorc*, *Slamf8*, and *Tbx1*) were not expressed at all and excluded from analysis to leave a 25 gene dataset (*B2m*, *Bcl6*, *Btla*, *Ccr7*, *Cd28*, *Cd40lg*, *Cd62l*, *Cd69*, *Cxcr5*, *Gapdh*, *Gata3*, *Gpr183*, *Icos*, *Il21*, *Il4*, *Il6ra*, *Il7r*, *Maf*, *Nr4a1*, *Pdcd1*, *Rgs16*, *Rn18s*, *S1pr2*, *Sh2d1a*, *Slamf6*). LimmaGP was used to identify differentially expressed genes between user-defined cell populations (based on micro-anatomical location), with a false discovery rate (FDR) of <0.05. To identify cell populations without a priori classification, we coupled NMF with a model selection method, NMFConsensus (Brunet et al., 2004) as implemented in GenePattern. Heatmaps were generated using the HeatMapViewer module in GenePattern and metagenes and vectors plotted in R (http://www.R-project.org). See also Supplemental Experimental Procedures.

Statistical Analysis

Data were analyzed with Prism software (GraphPad). See also Supplemental Experimental Procedures.

SUPPLEMENTAL INFORMATION

Supplemental Information includes seven figures, Supplemental Experimental Procedures, and seven movies and can be found with this article online at http://dx.doi.org/10.1016/j.immuni.2015.03.002.

AUTHOR CONTRIBUTIONS

T.G.P. conceptualized and designed the research; D.S., A.N., I.M., H.R.H., J.R.H., K.B., M.A., and T.G.P. performed experiments; M.T. and Y.M. provided KD mice; A.N. and W.K. performed bioinformatic analysis; A.N., I.M., T.C., and T.G.P. analyzed data; A.D.K., E.K.D., S.G.T., R.B., T.C., and T.G.P. interpreted data; A.N., I.M., T.C., and T.G.P. prepared figures and movies; and A.N., I.M., T.C., E.K.D., R.B., and T.G.P. prepared the manuscript.

ACKNOWLEDGMENTS

We thank T. Okada, J. Cyster, I. Grigorova, and D. Butt for helpful discussions and A. Basten and C. Sundling for comments on the manuscript. We thank P. Schwartzberg for SAP KO mice. We also thank J.-H. Cho for the primary T cell retroviral transduction protocol, N. Anders from the Small Animal Imaging Facility, R. Solomon and D. Snowden from the MLC Flow Cytometry Facility, and P. Bitter from the ACRF Facility. D.S. is supported by an NHMRC Postgraduate Scholarship, I.M. and H.R.H. by an Australian Post-graduate Award, S.G.T., A.D.K., and R.B. by Research Fellowships from the NHMRC and T.C. and T.G.P. by Career Development Fellowships from the NHMRC. This work was funded by Peter and Val Duncan, NHMRC Project Grants 1004632 (T.G.P.), 1062332 (T.C. and T.G.P.) and NHMRC Program Grant 1016953 (R.B. and S.G.T.). The contents of this article are solely the responsibility of the authors and do not reflect the views of NHMRC.

Received: September 16, 2014
Revised: November 24, 2014
Accepted: February 5, 2015
Published: March 31, 2015

REFERENCES

Allen, C.D., Okada, T., and Cyster, J.G. (2007). Germinal-center organization and cellular dynamics. Immunity *27*, 190–202.

Ansel, K.M., McHeyzer-Williams, L.J., Ngo, V.N., McHeyzer-Williams, M.G., and Cyster, J.G. (1999). In vivo-activated CD4 T cells upregulate CXC chemokine receptor 5 and reprogram their response to lymphoid chemokines. J. Exp. Med. *190*, 1123–1134.

Barral, P., Polzella, P., Bruckbauer, A., van Rooijen, N., Besra, G.S., Cerundolo, V., and Batista, F.D. (2010). CD169(+) macrophages present lipid antigens to mediate early activation of iNKT cells in lymph nodes. Nat. Immunol. *11*, 303–312.

Baumjohann, D., Okada, T., and Ansel, K.M. (2011). Cutting Edge: Distinct waves of BCL6 expression during T follicular helper cell development. J. Immunol. *187*, 2089–2092.

Breitfeld, D., Ohl, L., Kremmer, E., Ellwart, J., Sallusto, F., Lipp, M., and Förster, R. (2000). Follicular B helper T cells express CXC chemokine receptor 5, localize to B cell follicles, and support immunoglobulin production. J. Exp. Med. *192*, 1545–1552.

(F) The expression of the two metagenes, S1 (red) and S2 (black), as identified by NMF, are not associated with localization of secondary Tfh cells to the FM (green) or GC (orange).
(G) Re-ordering of the cells based on metagene expression reveals hidden clusters independent of their location.
(H) Cluster analysis of secondary Tfh cells showing metagene expression by single cells and the Euclidean distance between the centroid of the cells from the FM and GC groups.
(I) Vector contributions of each gene to metagene S1 and S2. Single cell data expression is pooled from two identical independent experiments.

Brunet, J.P., Tamayo, P., Golub, T.R., and Mesirov, J.P. (2004). Metagenes and molecular pattern discovery using matrix factorization. Proc. Natl. Acad. Sci. USA *101*, 4164–4169.

Cannons, J.L., Lu, K.T., and Schwartzberg, P.L. (2013). T follicular helper cell diversity and plasticity. Trends Immunol. *34*, 200–207.

Carrasco, Y.R., and Batista, F.D. (2007). B cells acquire particulate antigen in a macrophage-rich area at the boundary between the follicle and the subcapsular sinus of the lymph node. Immunity *27*, 160–171.

Chtanova, T., Tangye, S.G., Newton, R., Frank, N., Hodge, M.R., Rolph, M.S., and Mackay, C.R. (2004). T follicular helper cells express a distinctive transcriptional profile, reflecting their role as non-Th1/Th2 effector cells that provide help for B cells. J. Immunol. *173*, 68–78.

Chtanova, T., Han, S.J., Schaeffer, M., van Dooren, G.G., Herzmark, P., Striepen, B., and Robey, E.A. (2009). Dynamics of T cell, antigen-presenting cell, and pathogen interactions during recall responses in the lymph node. Immunity *31*, 342–355.

Chtanova, T., Hampton, H.R., Waterhouse, L.A., Wood, K., Tomura, M., Miwa, Y., Mackay, C.R., Brink, R., and Phan, T.G. (2014). Real-time interactive two-photon photoconversion of recirculating lymphocytes for discontinuous cell tracking in live adult mice. J Biophotonics *7*, 425–433.

Crotty, S. (2011). Follicular helper CD4 T cells (TFH). Annu. Rev. Immunol. *29*, 621–663.

Czar, M.J., Kersh, E.N., Mijares, L.A., Lanier, G., Lewis, J., Yap, G., Chen, A., Sher, A., Duckett, C.S., Ahmed, R., and Schwartzberg, P.L. (2001). Altered lymphocyte responses and cytokine production in mice deficient in the X-linked lymphoproliferative disease gene SH2D1A/DSHP/SAP. Proc. Natl. Acad. Sci. USA *98*, 7449–7454.

Dogan, I., Bertocci, B., Vilmont, V., Delbos, F., Mégret, J., Storck, S., Reynaud, C.A., and Weill, J.C. (2009). Multiple layers of B cell memory with different effector functions. Nat. Immunol. *10*, 1292–1299.

Estes, J.D., Thacker, T.C., Hampton, D.L., Kell, S.A., Keele, B.F., Palenske, E.A., Druey, K.M., and Burton, G.F. (2004). Follicular dendritic cell regulation of CXCR4-mediated germinal center CD4 T cell migration. J. Immunol. *173*, 6169–6178.

Garside, P., Ingulli, E., Merica, R.R., Johnson, J.G., Noelle, R.J., and Jenkins, M.K. (1998). Visualization of specific B and T lymphocyte interactions in the lymph node. Science *281*, 96–99.

Gatto, D., Paus, D., Basten, A., Mackay, C.R., and Brink, R. (2009). Guidance of B cells by the orphan G protein-coupled receptor EBI2 shapes humoral immune responses. Immunity *31*, 259–269.

Hale, J.S., Youngblood, B., Latner, D.R., Mohammed, A.U., Ye, L., Akondy, R.S., Wu, T., Iyer, S.S., and Ahmed, R. (2013). Distinct memory CD4+ T cells with commitment to T follicular helper- and T helper 1-cell lineages are generated after acute viral infection. Immunity *38*, 805–817.

Hardie, D.L., Johnson, G.D., Khan, M., and MacLennan, I.C. (1993). Quantitative analysis of molecules which distinguish functional compartments within germinal centers. Eur. J. Immunol. *23*, 997–1004.

Haynes, N.M., Allen, C.D., Lesley, R., Ansel, K.M., Killeen, N., and Cyster, J.G. (2007). Role of CXCR5 and CCR7 in follicular Th cell positioning and appearance of a programmed cell death gene-1high germinal center-associated subpopulation. J. Immunol. *179*, 5099–5108.

Hickman, H.D., Takeda, K., Skon, C.N., Murray, F.R., Hensley, S.E., Loomis, J., Barber, G.N., Bennink, J.R., and Yewdell, J.W. (2008). Direct priming of antiviral CD8+ T cells in the peripheral interfollicular region of lymph nodes. Nat. Immunol. *9*, 155–165.

Ise, W., Inoue, T., McLachlan, J.B., Kometani, K., Kubo, M., Okada, T., and Kurosaki, T. (2014). Memory B cells contribute to rapid Bcl6 expression by memory follicular helper T cells. Proc. Natl. Acad. Sci. USA *111*, 11792–11797.

Johnston, R.J., Poholek, A.C., DiToro, D., Yusuf, I., Eto, D., Barnett, B., Dent, A.L., Craft, J., and Crotty, S. (2009). Bcl6 and Blimp-1 are reciprocal and antagonistic regulators of T follicular helper cell differentiation. Science *325*, 1006–1010.

Junt, T., Moseman, E.A., Iannacone, M., Massberg, S., Lang, P.A., Boes, M., Fink, K., Henrickson, S.E., Shayakhmetov, D.M., Di Paolo, N.C., et al. (2007). Subcapsular sinus macrophages in lymph nodes clear lymph-borne viruses and present them to antiviral B cells. Nature *450*, 110–114.

Kastenmüller, W., Brandes, M., Wang, Z., Herz, J., Egen, J.G., and Germain, R.N. (2013). Peripheral prepositioning and local CXCL9 chemokine-mediated guidance orchestrate rapid memory CD8+ T cell responses in the lymph node. Immunity *38*, 502–513.

Kerfoot, S.M., Yaari, G., Patel, J.R., Johnson, K.L., Gonzalez, D.G., Kleinstein, S.H., and Haberman, A.M. (2011). Germinal center B cell and T follicular helper cell development initiates in the interfollicular zone. Immunity *34*, 947–960.

Kitano, M., Moriyama, S., Ando, Y., Hikida, M., Mori, Y., Kurosaki, T., and Okada, T. (2011). Bcl6 protein expression shapes pre-germinal center B cell dynamics and follicular helper T cell heterogeneity. Immunity *34*, 961–972.

Liu, Y.J., Oldfield, S., and MacLennan, I.C. (1988). Memory B cells in T cell-dependent antibody responses colonize the splenic marginal zones. Eur. J. Immunol. *18*, 355–362.

Liu, Y.J., Barthélémy, C., de Bouteiller, O., Arpin, C., Durand, I., and Banchereau, J. (1995). Memory B cells from human tonsils colonize mucosal epithelium and directly present antigen to T cells by rapid up-regulation of B7-1 and B7-2. Immunity *2*, 239–248.

Liu, X., Yan, X., Zhong, B., Nurieva, R.I., Wang, A., Wang, X., Martin-Orozco, N., Wang, Y., Chang, S.H., Esplugues, E., et al. (2012). Bcl6 expression specifies the T follicular helper cell program in vivo. J Exp Med *209*, 1841–1852, S1841-1824.

Lüthje, K., Kallies, A., Shimohakamada, Y., Belz, G.T., Light, A., Tarlinton, D.M., and Nutt, S.L. (2012). The development and fate of follicular helper T cells defined by an IL-21 reporter mouse. Nat. Immunol. *13*, 491–498.

MacLennan, I.C. (1994). Germinal centers. Annu. Rev. Immunol. *12*, 117–139.

Moriyama, S., Takahashi, N., Green, J.A., Hori, S., Kubo, M., Cyster, J.G., and Okada, T. (2014). Sphingosine-1-phosphate receptor 2 is critical for follicular helper T cell retention in germinal centers. J. Exp. Med. *211*, 1297–1305.

Nurieva, R.I., Chung, Y., Martinez, G.J., Yang, X.O., Tanaka, S., Matskevitch, T.D., Wang, Y.H., and Dong, C. (2009). Bcl6 mediates the development of T follicular helper cells. Science *325*, 1001–1005.

Okada, T., Miller, M.J., Parker, I., Krummel, M.F., Neighbors, M., Hartley, S.B., O'Garra, A., Cahalan, M.D., and Cyster, J.G. (2005). Antigen-engaged B cells undergo chemotaxis toward the T zone and form motile conjugates with helper T cells. PLoS Biol. *3*, e150.

Pape, K.A., Taylor, J.J., Maul, R.W., Gearhart, P.J., and Jenkins, M.K. (2011). Different B cell populations mediate early and late memory during an endogenous immune response. Science *331*, 1203–1207.

Paramithiotis, E., and Cooper, M.D. (1997). Memory B lymphocytes migrate to bone marrow in humans. Proc. Natl. Acad. Sci. USA *94*, 208–212.

Pereira, J.P., Kelly, L.M., Xu, Y., and Cyster, J.G. (2009). EBI2 mediates B cell segregation between the outer and centre follicle. Nature *460*, 1122–1126.

Phan, T.G., Gardam, S., Basten, A., and Brink, R. (2005). Altered migration, recruitment, and somatic hypermutation in the early response of marginal zone B cells to T cell-dependent antigen. J. Immunol. *174*, 4567–4578.

Phan, T.G., Grigorova, I., Okada, T., and Cyster, J.G. (2007). Subcapsular encounter and complement-dependent transport of immune complexes by lymph node B cells. Nat. Immunol. *8*, 992–1000.

Phan, T.G., Green, J.A., Gray, E.E., Xu, Y., and Cyster, J.G. (2009). Immune complex relay by subcapsular sinus macrophages and noncognate B cells drives antibody affinity maturation. Nat. Immunol. *10*, 786–793.

Plotkin, S.A. (2008). Vaccines: correlates of vaccine-induced immunity. Clin. Infect. Dis. *47*, 401–409.

Rasheed, A.U., Rahn, H.P., Sallusto, F., Lipp, M., and Müller, G. (2006). Follicular B helper T cell activity is confined to CXCR5(hi)ICOS(hi) CD4 T cells and is independent of CD57 expression. Eur. J. Immunol. *36*, 1892–1903.

Roozendaal, R., Mempel, T.R., Pitcher, L.A., Gonzalez, S.F., Verschoor, A., Mebius, R.E., von Andrian, U.H., and Carroll, M.C. (2009). Conduits mediate

transport of low-molecular-weight antigen to lymph node follicles. Immunity *30*, 264–276.

Schaerli, P., Willimann, K., Lang, A.B., Lipp, M., Loetscher, P., and Moser, B. (2000). CXC chemokine receptor 5 expression defines follicular homing T cells with B cell helper function. J. Exp. Med. *192*, 1553–1562.

Schaerli, P., Loetscher, P., and Moser, B. (2001). Cutting edge: induction of follicular homing precedes effector Th cell development. J. Immunol. *167*, 6082–6086.

Shulman, Z., Gitlin, A.D., Targ, S., Jankovic, M., Pasqual, G., Nussenzweig, M.C., and Victora, G.D. (2013). T follicular helper cell dynamics in germinal centers. Science *341*, 673–677.

Talay, O., Yan, D., Brightbill, H.D., Straney, E.E., Zhou, M., Ladi, E., Lee, W.P., Egen, J.G., Austin, C.D., Xu, M., and Wu, L.C. (2012). IgE^{+} memory B cells and plasma cells generated through a germinal-center pathway. Nat. Immunol. *13*, 396–404.

Tangye, S.G., Ma, C.S., Brink, R., and Deenick, E.K. (2013). The good, the bad and the ugly - TFH cells in human health and disease. Nat. Rev. Immunol. *13*, 412–426.

Victora, G.D., and Nussenzweig, M.C. (2012). Germinal centers. Annu. Rev. Immunol. *30*, 429–457.

Victora, G.D., Schwickert, T.A., Fooksman, D.R., Kamphorst, A.O., Meyer-Hermann, M., Dustin, M.L., and Nussenzweig, M.C. (2010). Germinal center dynamics revealed by multiphoton microscopy with a photoactivatable fluorescent reporter. Cell *143*, 592–605.

Weber, J.P., Fuhrmann, F., and Hutloff, A. (2012). T-follicular helper cells survive as long-term memory cells. Eur. J. Immunol. *42*, 1981–1988.

Yu, D., Rao, S., Tsai, L.M., Lee, S.K., He, Y., Sutcliffe, E.L., Srivastava, M., Linterman, M., Zheng, L., Simpson, N., et al. (2009). The transcriptional repressor Bcl-6 directs T follicular helper cell lineage commitment. Immunity *31*, 457–468.